Colloid Polym Sci (2012) 290:1759–1764
DOI 10.1007/s00396-012-2715-x

ORIGINAL CONTRIBUTION

Architecture-adapted raspberry-like gold@polyaniline particles: facile synthesis and catalytic activity

Xiaobin Xu · Xianchun Liu · Qun Yu · Wei Wang · Shuangxi Xing

Received: 5 March 2012 / Revised: 25 May 2012 / Accepted: 14 June 2012 / Published online: 3 July 2012

Abstract A facile route was introduced to generate uniform raspberry-like gold@polyaniline (AuNP@PANI) particles in the presence of sodium dodecylsulfate (SDS). The surfactant SDS played an important role in both generating a uniform structure and stabilizing these particles. Upon addition of low-molecular weight organics, the regulation on the gold architecture was realized from a compact to stretched configuration owing to the change of surface tension and a possible swell process. The catalytic activity of the raspberry-like AuNP@PANI was investigated using the reduction of 4-nitrophenol by $NaBH_4$ and electrocatalytic oxidation of glucose as model reactions. It was found that the AuNP @PANI particles with the most stretched architecture presented the highest catalytic activity owing to their largest contact surface to the reactants.

Keywords gold@polyaniline · Raspberry-like structure · Low-molecular weight organics · Catalytic activity

Introduction

Noble metal micro/nanostructures with specific morphology have received considerable attention owing to their potential applications in optics, catalysis, sensors, surface-enhanced Raman scattering, and biology [1–5]. The formation of unique metal structures leads to the generation of novel properties, especially when their size and shape are highly controllable. Therefore, to construct a simple system for the preparation of such metal structures has always been pursued. Of great interest and significance, the raspberry-like metal particles present high surface area and sufficient adsorption sites, which render them excellent catalytic performance and sensor ability [6–8]. Furthermore, introducing conducting polymers into such metal systems is an exciting topic to design functional architectures [9], where conducting polymers may serve as electroactive linkers among the metal particles [10]. To date, many strategies have been designed for the generation of metal/conducting polymers micro/nanostructures, including ligand exchange [11], self-assembly [6, 7, 12–15], and seeded growth [16, 17]. Even so, a facile route is still urgently required to achieve uniform and size-tunable metal/conducting polymers structures.

Here, we report the synthesis of uniform raspberry-like gold@polyaniline (AuNP@PANI) particles by a simple method: mix the ingredients in right ratio at room temperature followed by incubation for a period of time. In particular, addition of low-molecular weight organics into the system can effectively regulate on the morphology of the resulting structures. Their catalytic property differs from each other depending on the different architectures. In addition, owing to the protection of the thin PANI layer, the catalysts keep almost unchanged after recycled, making it promising to be reused reasonably.

Electronic supplementary material The online version of this article (doi:10.1007/s00396-012-2715-x) contains supplementary material, which is available to authorized users.

X. Xu · X. Liu · S. Xing (✉)
Faculty of Chemistry, Northeast Normal University, Changchun 130024, People's Republic of China
e-mail: xingsx737@nenu.edu.cn

Q. Yu · W. Wang
College of Electronic Science and Engineering, Jilin University, Changchun 130012, People's Republic of China

Experimental

Preparation of AuNP@PANI

To prepare the raspberry-like AuNP@PANI particles, aniline (100 mM, 1 mL), sodium dodecylsulfate (SDS, 40 mM,

1 mL), $HAuCl_4$ (2.94 mM, 1 mL), and 1 mL of water were mixed followed by shaking vigorously for 5 s and incubation for 4 h at room temperature. The total volume of the reagents was 4 mL, where [aniline]=25 mM, [SDS]=10 mM, [$HAuCl_4$]=0.74 mM. The addition of water was for the sake of comparing with other experiments where ethanol or acetone was used as additives. The color of the aniline/SDS solution turned from wine red to brown upon addition of $HAuCl_4$, and finally into dark green, revealing the realization of a fast redox process between aniline and $HAuCl_4$. The product was purified by centrifugation at 8,000 rpm for 5 min to remove the excessive monomers or polymers. After removal of the supernatant, the isolated particles were dispersed into diluted SDS (3.6 mM) solution for further investigation.

In the case of addition of additives, the water in the above system was replaced by 1 mL of ethanol or acetone under otherwise the same conditions.

Catalytic reaction for degradation of 4-nitrophenol

The catalytic reactions for degradation of 4-nitrophenol (4-NP) was conducted as follows: 400 μL of as-prepared solution was concentrated to a total of 10 μL by centrifugation at 8,000 rpm for 5 min. After removal of the supernatant, the isolated AuNP@PANI particles was immediately added to a freshly prepared reaction mixture (3 mL) containing 4-NP (0.15 mM) and $NaBH_4$ (5.5 mM). The optical property of the reaction system was analyzed by using a UV–vis spectroscopy at every 5 min interval. As for the investigation on the catalytic activity of the products from a system with addition of ethanol or acetone, the same amount of reaction mixture was extracted.

Electrocatalytic oxidation of glucose

A piece of indium–tin–oxide (ITO)-coated glass (1×5 cm) was firstly precleaned with acetone and immersed into a solution of $H_2O_2/NH_3{\cdot}H_2O/H_2O$ (1:1:5 *v*/*v*) for 30 min. After that, the ITO glass was rinsed with de-ionized water and dried at 40 °C. Of the as-prepared AuNP@PANI solutions, 400 μL were centrifuged, dipped on the cleaned ITO glass evenly, and dried in air to form thin films.

The electrocatalytic oxidation of glucose was performed on a CHI 660D electrochemical workstation (CH Instruments, Chenhua Co., Shanghai, China). A conventional three-electrode cell was utilized with a saturated Ag/AgCl electrode as the reference electrode, a platinum plate as the counter electrode, and the AuNP@PANI-loaded ITO glass as the working electrode. A potential scan in the range of −0.4 to 1.1 V with a scan rate of 50 mV s^{-1} was implemented to explore the electrochemical behavior of glucose in stirred 0.1 M NaOH aqueous solutions containing 0.67 mM glucose.

The estimation of the electrochemically active surface area of the raspberry-like AuNP@PANI gold electrodes were carried out using cyclic voltammetry and the Randles–Sevcik equation for a reversible redox couple, which at 25 °C is [18]

$$I_p = \left(2.69 \times 10^5\right) n^{3/2} \mathrm{AD}^{1/2} \nu^{1/2} C_\infty$$

where I_p is the peak current (*A*), *n* is the number of electrons transferred, *A* is the electrode area (square centimeters), *D* is the diffusion coefficient of the electroactive species (square centimeters per second), ν is the scan rate (volts per second), and C_∞ is the bulk concentration of the same electroactive species (mole per cubic centimeter). Here, we used 5 mM $K_3Fe(CN)_6$ in 0.1 M KCl aqueous solution for this purpose, and $K_3Fe(CN)_6$ has a diffusion coefficient of 1.0×10^{-5} cm^2 s^{-1} at 25 °C. The scan rate kept at 50 mV s^{-1} in the measurement.

Characterization

The morphology of the products was investigated by a high resolution transmission electron microscopy (HRTEM, JEOL-2100F) operated at 200 kV. In the typical sample, $(NH_4)_6Mo_7O_{24}$ (3.4 mM) was used as the negative stain to improve contrast for the transmission electron microscopy (TEM) image of the core–shell structure. Ultraviolet–visible (UV–vis) spectra were collected on a UV-2550 spectrophotometer. Raman spectrum was collected from the sample solution (isolated AuNP@PANI dispersed in diluted SDS solution) in a 4-mL glass vial on a PeakSeeker Pro spectrometer (Raman Systems Inc.) using a red laser (λ=785 nm) at 290 mW.

Results and discussion

Figure 1a shows the TEM image of the as-synthesized AuNP@PANI particles. These particles appear raspberry-like shape with an average diameter of 98±8 nm. A closer detection demonstrates they are composed by many smaller fiber-like gold nanoparticles (AuNPs, d_{av}=14±2 nm in length, 8±2 nm in width; Fig. 1b). Besides, a thin layer of polymer about 2 nm encapsulates these particles, which can effectively prevent them from further aggregation [19, 20]. The UV–vis spectrum confirms the formation of AuNP and PANI (Fig. 1c). The peak at 556 nm originates from the surface plasmon resonance of the gold particles and the peak around 400 nm can be assigned to the polaron-π* of PANI [21]. Figure 1d gives the Raman spectrum of the isolated raspberry-like AuNP@PANI. The characteristic peaks at 1,599, 1,492, and 1,180 cm^{-1} confirm the formation of PANI

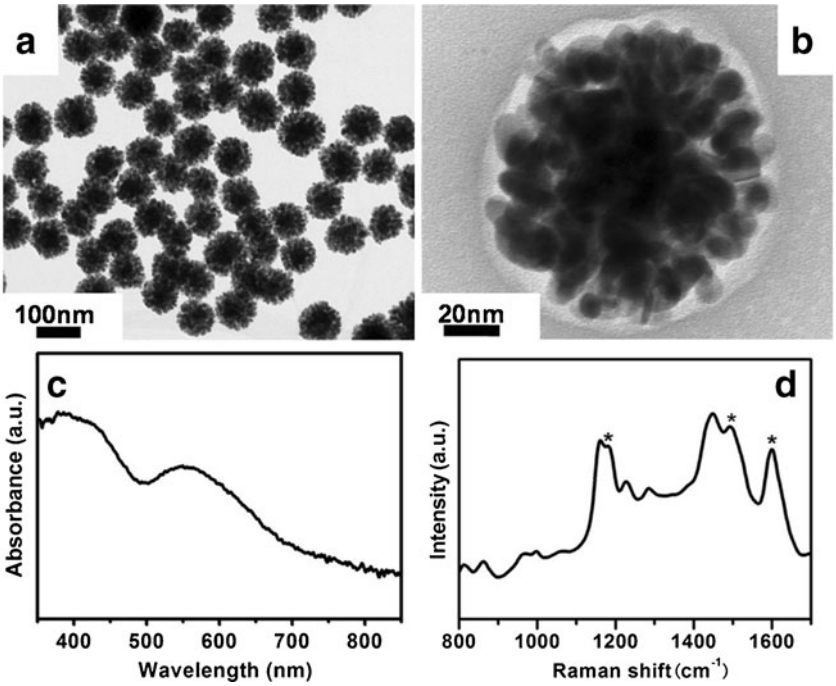

Fig. 1 **a**, **b** TEM images of typical raspberry-like AuNP@-PANI particles at low and high magnification (negative stain was used in **b**); **c** UV–vis and **d** Raman spectrum of the purified raspberry-like AuNP@PANI particles

on the surface of gold [20]. The surfactant SDS plays an important role in the overall synthesis. When the SDS concentration is decreased to 2 mM, a broad size distribution is observed (Fig. 2a).

We believe the SDS molecules entrap into the PANI structure and provide electronic repulsion on the surface of the polymer shell [19, 20, 22]. When such repulsion is deficient, aggregation inevitably occurs. This can be further confirmed by another control experiment where no surfactant is used. In this system, due to the high surface energy of the AuNPs, only fiber-like gold aggregates with length up to 600 nm are observed (Fig. 2b).

Similar structured gold particles have been reported previously [12, 16]. In our system, we consider the redox reaction between $HAuCl_4$ and aniline leads to the nucleation of Au^0 and the formation of PANI simultaneously, followed by a spontaneous assembly process. During the dynamic growth, smaller AuNPs tend to aggregate owing to their high surface activity. Meanwhile, PANI entrapped with SDS covers the surface of gold aggregates to further decrease the total surface energy. As a result, raspberry-like gold structures are achieved.

Addition of low-molecular weight organics, such as ethanol and acetone can lead to an increase in the particle size, as shown in Fig. 3. The mean diameter of the obtained particles increases from 98 to 184 and 248 nm with addition of 1 mL of ethanol and acetone instead of water, respectively (Fig. 3a and b). Moreover, these particles present stretched configuration, indicating a swell process may exist during the particle formation process. To confirm this assumption, the as-synthesized particles from the system without organics are centrifuged and incubated in ethanol overnight. As a result, an increment of particle size is observed (from 98 to 135 nm, Fig. 3c). The post-swelling process did not produce branches as stretching as those synthesized in the later two systems. We consider once PANI was formed, they cannot extend too much. Thus, a side effect for the formation of highly stretched PANI may originate from the good solubility of aniline/PANI in the

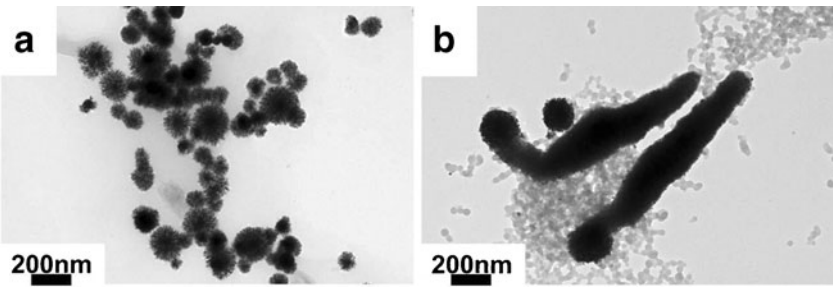

Fig. 2 TEM image of AuNP@PANI particles from a water system **a** containing 2 mM SDS and **b** in the absence of SDS

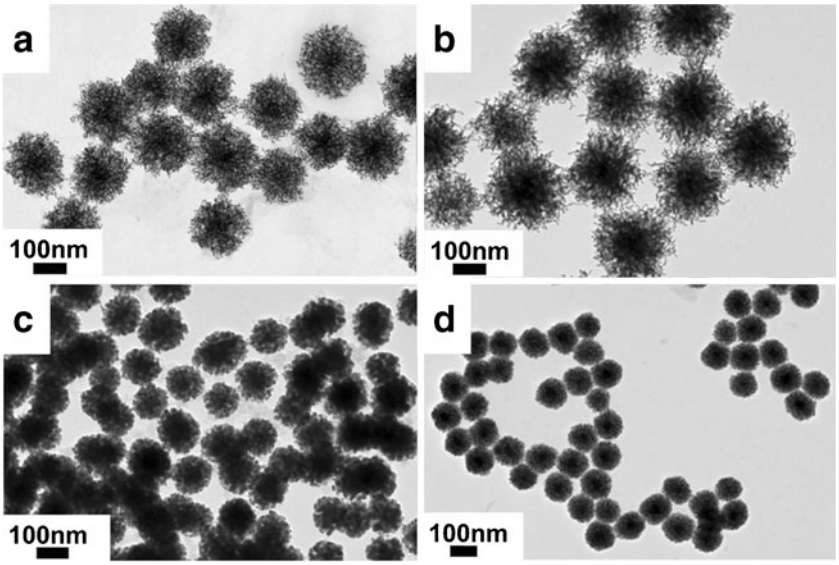

Fig. 3 TEM images of raspberry-like Au@PANI particles upon addition of 1 mL of **a** ethanol and **b** acetone; **c** TEM image of the typical raspberry-like Au@PANI particles after incubation in ethanol overnight; **d** TEM image of raspberry-like Au@PANI particles upon addition of 0.2 mL of ethanol

mixed solvent, and the stretched PANI formed during synthesis also occurred.

The surface tension should be another driving force to make the expansion of the AuNP@PANI particles. In water media, owing to their high surface tension, the AuNPs prior to form a close packing state to avoid large exposure to water. Upon addition of ethanol, the interface energy between the gold/PANI particles and the surrounding is greatly reduced and the AuNPs have the tendency to relieve themselves from the high strain and a more stretched assembly configuration is thus obtained. In this sense, as the content of ethanol changed, the size of the particles will alter accordingly. The average diameter of the particles is 122 nm for addition of 0.2 mL of ethanol and it increases to 184 nm for 1 mL of ethanol (Fig. 3a and d). Furthermore, acetone can reduce the interface energy in larger degree compared to that of ethanol. Consequently, a larger particle with much more loose packing state is achieved when acetone is introduced (Fig. 3b).

The raspberry-like structure may render the AuNP @PANI particles with high catalytic activity. PANI plays an important role in the catalytic, especially the electrocatalytic process. On one hand, the existence of PANI improves the dispersity and stability of AuNPs. On the other hand, small-sized catalysts are able to provide high activity for a special reaction; however, if they are separated by each other, a redox reaction may be blocked with the oxidation and reduction half reactions occurring individually. Therefore, a good electrical connection between these small catalysts

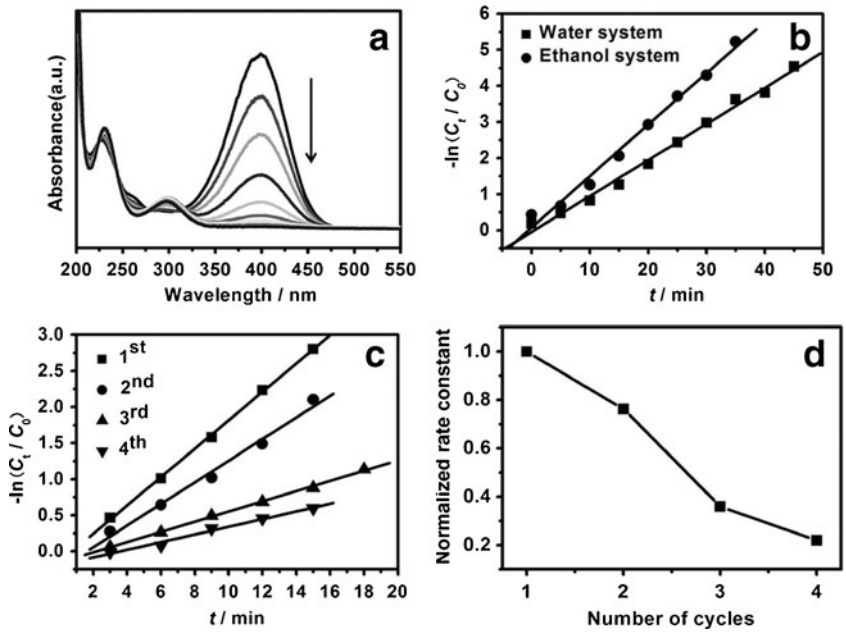

Fig. 4 **a** A typical time-dependent evolution of UV–vis absorption spectra using the raspberry-like AuNP@PANI particles; **b** the relationship between $-\ln (C_t/C_0)$ versus time (t) in water and ethanol system, and the slope of the linear fit represents the rate constant (k); **c** The relationship between $-\ln (C_t/C_0)$ versus time in different cycle numbers; **d** dependence of normalized k on cycle numbers

is of great importance [23, 24]. The raspberry-like AuNP @PANI meets well with the above requirement, where the smaller AuNPs are assembled with the linkage of PANI shell (Fig. 1b). Furthermore, the PANI protects the AuNPs from aggregation in the catalytic process (vide infra). Attention should be paid that the PANI shell allows the penetration of the reactants to contact with the AuNPs, consistent with our previous reports on the formation of (Au@Ag) @PPy [19] and (Au@Ag)@PANI [22] systems, where the polymer monomer and Ag^+ could reach the Au seeds surface through the polymer shell.

After introducing ethanol and acetone, the morphology of the products were altered, which may take great influence on their catalytic activity. Comparing Fig. 3a and b with 1a, one can see the compact "cores" of the particle in the typical water system become smaller and more elongated branches are formed, turning to a more stretched structure when ethanol and acetone are involved. These allow the AuNPs in the later two systems have greater chance to contact and react with the reaction mixture.

In order to illustrate the results conveniently, we define systems 1, 2, and 3 (abbreviated to S1, S2, and S3) as the system with addition of 1 ml of water, ethanol, and acetone, respectively.

To prove our assumption that the catalytic activity is dependent on the morphology and structure of the particles, we used the reduction of 4-NP to 4-aminophenol (4-AnP) by $NaBH_4$ in aqueous media as a model reaction. Upon addition of the raspberry-like AuNP@PANI particles, the absorption intensity of the 4-NP at 399 nm decreases quickly and a new absorption band at 297 nm is gradually developed, corresponding to the formation of the 4-AnP. The pure PANI does not have catalytic activity on the reduction of 4-NP to 4-AnP (Fig. S10), further confirming the penetration of the reactants through the polymer shell to the Au surface. Figure 4a is a typical time-dependent evolution of UV–vis absorption spectra using the raspberry-like AuNP@PANI particles.

Using the sample obtained from S1, a complete degradation in 45 min was achieved (Fig. S11). Considering this reaction a pseudo-first-order reaction (the concentration of BH_4^- greatly exceeds that of 4-NP), the rate constant (k) is determined by the slope of the linear fit of $-\ln(C_t/C_0)$ versus time, where C_t/C_0 represents the ratio of 4-NP concentrations at time t and 0 as calculated based on their corresponding absorption intensity in the kinetic UV-Vis spectra (Fig. S12). A k value of 0.9976 min^{-1} is thus calculated. A larger value of k (1.427 min^{-1}) is obtained from S2 (Fig. 4b). The catalytic activity of S2 is 43 % larger than that of the S1, confirming our previous assumption.

As for the products from S3, they should display the highest catalytic activity based on our previous discussion and the conclusion above. However, by using these particles, no significant changes of the peak intensity at 399 nm can be detected in a certain period of time, that is, 4-NP is hardly degraded. $NaBH_4$ as a widely used reductant can convert ketones and aldehydes to alcohols. In S3, $NaBH_4$ react with acetone to generate isopropyl alcohol, which takes negative effects on the catalytic reaction. This also confirms the swell process for the morphology changes with addition of organics that acetone may exist in the final product to keep a swollen structure.

We further studied the recycled behavior of the catalysts using this reaction. The catalytic degradation effect ($-\ln C_t/C_0$) as a function of time on different cycle numbers is presented in Fig. 4c. Based on the above result, the corresponding rate constants are achieved (Fig. 4d). After four cycles, the catalyst still kept its activity although a decreasing effect was detected and we consider this should be largely attributed to the centrifuge loosing. This good performance should be related to the protection of the PANI shell, which priors to maintain the well-defined gold structures and keep it from aggregation. From the TEM image of the catalyst centrifuged after four cycles (Fig. S18), one can see that the raspberry-like structure remains unchanged except for a bit aggregation, which originates from the decreased SDS concentration [19, 20]. In contrast, the normalized catalytic activity of citrate-stabilized AuNPs is reduced to 21.97 % after the first cycle.

In order to rule out the influence of acetone on the above reduction process, we carried out the electrocatalytic oxidation of glucose by using these particles from S1, S2 and S3.

Figure 5 shows the CV curves of the glucose oxidation by using AuNP@PANI particles obtained from S1, S2 and S3 as catalysts. Similar to the previous reports, in each anodic current curve, there are two major oxidation peaks except the position shift, which perhaps attributes to the presence of PANI. In the positive scan of potential, the peaks at *ca*. 0.1 and 0.7 V correspond to the oxidation of glucose and the further oxidation of gluconolactone, respectively [25, 26]. Comparing the three curves, we can see the

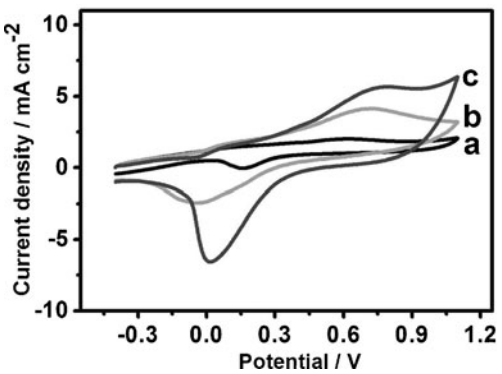

Fig. 5 Cyclic voltammograms for the oxidation of glucose (0.67 mM) at AuNP@PANI from water system S1 (*a*), ethanol system S2 (*b*) and acetone system S3 (*c*) electrodes in 0.1 M NaOH at 50 mV s^{-1}

catalyst obtained from S1 generates a maximum anodic current density of 2.03 mA cm^{-2} (at the peak potential of 0.61 V), whereas the catalysts from S2 and S3 yield a current density of 4.11 (at the peak potential of 0.71 V) and 5.71 mA cm^{-2} (at the peak potential of 0.79 V), respectively. This agrees well with our former discussion that the AuNP@PANI particles from the system containing acetone with a much more stretched structure present the highest catalytic activity.

Conclusions

In summary, we provided a straightforward route to synthesize raspberry-like gold particles that were encapsulated and protected by thin polyaniline layers. Addition of low-molecular weight organics led to the facile regulation on the architecture of the products. The catalytic activity of these particles varied based on their corresponding morphologies and components. Such size-tunable particles with high uniform morphology make them as promising materials for optical crystals, catalysis, and electronic devices.

Acknowledgments The authors thank the National Natural Science Foundation of China (grant no. 21103018) and Jilin Provincial Science and Technology Development Foundation (grant no. 201101010) for financial support.

References

1. Cortie MB, McDonagh AM (2011) Synthesis and optical properties of hybrid and alloy plasmonic nanoparticles. Chem Rev 111:3713–3735. doi:10.1021/cr1002529
2. Daniel M-C, Astruc D (2003) Gold nanoparticles: assembly, supramolecular chemistry, quantum-size-related properties, and applications toward biology, catalysis, and nanotechnology. Chem Rev 104:293–346. doi:10.1021/cr030698+
3. Ray PC (2010) Size and shape dependent second order nonlinear optical properties of nanomaterials and their application in biological and chemical sensing. Chem Rev 110:5332–5365. doi:10.1021/cr900335q
4. Hartland GV (2011) Optical studies of dynamics in noble metal nanostructures. Chem Rev 111:3858–3887. doi:10.1021/cr1002547
5. Yuan Q, Wang X (2010) Aqueous-based route toward noble metal nanocrystals: morphology-controlled synthesis and their applications. Nanoscale 2:2328–2335. doi:10.1039/c0nr00342e
6. Guo S, Dong S, Wang E (2008) Monodisperse raspberry-like gold submicrometer spheres: large-scale synthesis and interface assembling for colloid sphere array. Cryst Growth Des 8:3581–3585. doi:10.1021/cg800023d
7. Shen Q, Jiang L, Zhang H, Min Q, Hou W, Zhu J-J (2008) Three-dimensional dendritic pt nanostructures: sonoelectrochemical synthesis and electrochemical applications. J Phys Chem C 112:16385–16392. doi:10.1021/jp8060043
8. Kawasaki JK, Arnold CB (2011) Synthesis of platinum dendrites and nanowires via directed electrochemical nanowire assembly. Nano Lett 11:781–785. doi:10.1021/nl1039956
9. Mallick K, Mondal K, Witcomb M, Scurrell M (2008) Gas phase hydrogenation reaction using a 'metal nanoparticle–polymer' composite catalyst. J Mater Sci 43:6289–6295. doi:10.1007/s10853-008-2892-7
10. Hosseini M, Momeni M, Faraji M (2010) Electrochemical fabrication of polyaniline films containing gold nanoparticles deposited on titanium electrode for electro-oxidation of ascorbic acid. J Mater Sci 45:2365–2371. doi:10.1007/s10853-009-4202-4
11. Sajanlal PR, Sreeprasad TS, Nair AS, Pradeep T (2008) Wires, plates, flowers, needles, and core-shells: diverse nanostructures of gold using polyaniline templates. Langmuir 24:4607–4614. doi:10.1021/la703593c
12. Shiigi H, Yamamoto Y, Yoshi N, Nakao H, Nagaoka T (2006) One-step preparation of positively-charged gold nanoraspberry. Chem Commun 42:4288–4290. doi:10.1039/b610085f
13. Kun H et al (2006) One-step synthesis of 3D dendritic gold/polypyrrole nanocomposites via a self-assembly method. Nanotechnology 17:283. doi:10.1088/0957-4484/17/1/048
14. Mallick K, Witcomb MJ, Dinsmore A, Scurrell MS (2005) Fabrication of a metal nanoparticles and polymer nanofibers composite material by an in situ chemical synthetic route. Langmuir 21:7964–7967. doi:10.1021/la050534j
15. Sharma M, Ambolikar A, Aggarwal S (2011) In situ synthesis of gold–polyaniline composite in nanopores of polycarbonate membrane. J Mater Sci 46:5715–5722. doi:10.1007/s10853-011-5525-5
16. Pan M, Xing S, Sun T, Zhou W, Sindoro M, Teo HH, Yan Q, Chen H (2010) 3D dendritic gold nanostructures: seeded growth of a multi-generation fractal architecture. Chem Commun 46:7112–7114. doi:10.1039/c0cc00820f
17. Song Y, Yang Y, Medforth CJ, Pereira E, Singh AK, Xu H, Jiang Y, Brinker CJ, van Swol F, Shelnutt JA (2003) Controlled Synthesis of 2-D and 3-D Dendritic Platinum Nanostructures. J Am Chem Soc 126:635–645. doi:10.1021/ja037474t
18. Gooding JJ, Praig VG, Hall EAH (1998) Platinum-catalyzed enzyme electrodes immobilized on gold using self-assembled layers. Anal Chem 70:2396–2402. doi:10.1021/ac971035t
19. Xing S, Tan LH, Chen T, Yang Y, Chen H (2009) Facile fabrication of triple-layer (Au@Ag)@polypyrrole core-shell and (Au@H_2O)@polypyrrole yolk-shell nanostructures. Chem Commun 45:1653–1654. doi:10.1039/b821125f
20. Xing S, Tan LH, Yang M, Pan M, Lv Y, Tang Q, Yang Y, Chen H (2009) Highly controlled core/shell structures: Tunable conductive polymer shells on gold nanoparticles and nanochains. J Mater Chem 19:3286–3291. doi:10.1039/b900993k
21. MacDiarmid AG, Epstein AJ (1994) The concept of secondary doping as applied to polyaniline. Synth Met 65:103–116. doi:10.1016/0379-6779(94)90171-6
22. Xing S, Feng Y, Tay YY, Chen T, Xu J, Pan M, He J, Hng HH, Yan Q, Chen H (2010) Reducing the symmetry of bimetallic Au@Ag nanoparticles by exploiting eccentric polymer shells. J Am Chem Soc 132:9537–9539. doi:10.1021/ja102591z
23. Zeng J, Zhang Q, Chen J, Xia Y (2009) A comparison study of the catalytic properties of Au-based nanocages, nanoboxes, and nanoparticles. Nano Lett 10:30–35. doi:10.1021/nl903062e
24. Granot E, Katz E, Basnar B, Willner I (2005) Enhanced bioelectrocatalysis using Au-nanoparticle/polyaniline hybrid systems in thin films and microstructured rods assembled on electrodes. Chem Mater 17:4600–4609. doi:10.1021/cm050193v
25. Wang J, Gong J, Xiong Y, Yang J, Gao Y, Liu Y, Lu X, Tang Z (2011) Shape-dependent electrocatalytic activity of monodispersed gold nanocrystals toward glucose oxidation. Chem Commun 47:6894–6896. doi:10.1039/c1cc11784j
26. Tominaga M, Shimazoe T, Nagashima M, Taniguchi I (2005) Electrocatalytic oxidation of glucose at gold nanoparticle-modified carbon electrodes in alkaline and neutral solutions. Electrochem Commun 7:189–193. doi:10.1016/j.elecom.2004.12.006